diagnostics

MDPI

Article

Detection of Tumour-Targeted IRDye800CW Tracer with Commercially Available Laparoscopic Surgical Systems

Daan J. Sikkenk [1,2,†], Andrea J. Sterkenburg [3,†], Iris Schmidt [3], Dimitris Gorpas [4,5], Wouter B. Nagengast [3] and Esther C. J. Consten [1,2,*]

1 Department of Surgery, University Medical Centre Groningen, University of Groningen, Hanzeplein 1, 9713 GZ Groningen, The Netherlands
2 Department of Surgery, Meander Medical Centre, Maatweg 3, 3813 TZ Amersfoort, The Netherlands
3 Department of Gastroenterology, University Medical Centre Groningen, University of Groningen, Hanzeplein 1, 9713 GZ Groningen, The Netherlands
4 Institute of Biological and Medical Imaging, Helmholtz Zentrum München (GmbH), Ingolstädter Landstraße 1, D-85764 Neuherberg, Germany
5 Chair of Biological Imaging, Center for Translational Cancer Research (TranslaTUM), Technical University of Munich, Ismaninger Straße 22, D-81675 Munich, Germany
* Correspondence: e.c.j.consten@umcg.nl
† These authors contributed equally to this work.

Abstract: (1) Introduction: Near-infrared fluorescence (NIRF) combined with tumour-targeted tracers, such as bevacizumab-800CW, could aid surgical decision-making. This study explored the use of IRDye800CW, conjugated to bevacizumab, with four commercially available NIRF laparoscopes optimised for indocyanine green (ICG). (2) Methods: A (lymph node) phantom was made from a calibration device for NIRF and tissue-mimicking material. Serial dilutions of bevacizumab-800CW were made and ICG functioned as a reference. System settings, working distance, and thickness of tissue-mimicking material were varied to assess visibility of the fluorescence signal and tissue penetration. Tests were performed with four laparoscopes: VISERA ELITE II, Olympus; IMAGE1 S™ 4U Rubina, KARL STORZ; ENDOCAM Logic 4K platform, Richard Wolf; da Vinci Xi, Intuitive Surgical. (3) Results: The lowest visible bevacizumab-800CW concentration ranged between 13–850 nM (8–512 times diluted stock solution) for all laparoscopes, but the tracer was not visible through 0.8 cm of tissue in all systems. In contrast, ICG was still visible at a concentration of 0.4 nM (16,384 times diluted) and through 1.6–2.4 cm of tissue. Visibility and tissue penetration generally improved with a reduced working distance and manually adjusted system settings. (4) Conclusion: Depending on the application, bevacizumab-800CW might be sufficiently visible with current laparoscopes, but optimisation would widen applicability of tumour-targeted IRDye800CW tracers.

Keywords: fluorescence guided surgery; fluorescence molecular imaging; image-guided surgery; near-infrared fluorescence (NIRF); targeted tracer; IRDye800CW; indocyanine green (ICG)

check for updates

Citation: Sikkenk, D.J.; Sterkenburg, A.J.; Schmidt, I.; Gorpas, D.; Nagengast, W.B.; Consten, E.C.J. Detection of Tumour-Targeted IRDye800CW Tracer with Commercially Available Laparoscopic Surgical Systems. *Diagnostics* **2023**, *13*, 1591. https://doi.org/10.3390/diagnostics13091591

Academic Editor: Antonio Maccio

Received: 30 March 2023
Revised: 22 April 2023
Accepted: 27 April 2023
Published: 29 April 2023

Copyright: © 2023 by the authors. Licensee MDPI, Basel, Switzerland. This article is an open access article distributed under the terms and conditions of the Creative Commons Attribution (CC BY) license (https://creativecommons.org/licenses/by/4.0/).

1. Introduction

Surgeons rely on visual and tactile feedback for intraoperative decision-making. However, many laparoscopic or robotic surgical systems lack tactile feedback. Image-guided surgery, such as near-infrared fluorescence (NIRF), aid surgical decision-making with additional visual feedback. There has been an increasing interest in NIRF and its new applications for fluorescence guided surgery. In oncological surgery, NIRF is primarily used to achieve tumour-free excision, identify occult lesions, debulking, and recognition of vital structures [1].

Near-infrared light (650–950 nm for the first NIRF window) has superior tissue penetration compared to white light and has limited interference with human tissues [2–5]. Fluorescence-guided surgery is primarily focused on the non-specific tracer indocyanine green (ICG) as it has a well-established safety profile and is the only FDA and EMA approved

fluorophore for general surgery [6]. Development of new fluorescent tracers is mostly focused on tumour-targeted tracers; fluorophores bound to a ligand [7,8]. Tumour-targeted tracers could provide real-time information about the presence of tumour or metastases and allow intraoperative decision-making [9]. Furthermore, antibodies are commonly used as a ligand due to their availability for a wide range of targets and modifiability [10].

The fluorophore IRDye800CW has an NH ester group for labelling proteins such as antibodies [11], making it an applicable fluorophore for tumour-targeted tracers. By using the same fluorophore for multiple antibodies, the same camera system could be used for a wide variety of tumour-targeted tracers and indications. Multiple commercially available open-air NIRF camera systems can detect IRDye800CW (absorption: ~780 nm, excitation: ~800 nm [11,12]), but are primarily intended for ICG (absorption: ~800 nm, excitation: ~830 nm [13]) and cannot be used for minimally invasive surgery [14]. Bevacizumab-800CW is a tumour-targeted tracer, aimed at vascular endothelial growth factor α (VEGFα), which has been used in multiple clinical studies [9,15–22]. Likewise, cetuximab-800CW, aimed at endothelial growth factor, is used in multiple clinical trials [23,24], and various other antibodies conjugated to IRDye800CW are currently investigated [25–27] since the process of developing these tracers is relatively simple compared to developing a new investigational drug or tracer [27,28]. Micro-dosages of tumour-targeted tracers are most often used in studies since first-in-patient studies can more easily be conducted due to the unlikelihood of major side effects [29–32]. Simultaneously, tumour-targeted tracers in micro-dosages still provide sufficient fluorescent intensity for diagnostic purposes.

Our intention is to use targeted tracers for the detection of sentinel lymph nodes or lymph node metastases in patients with colon cancer during laparoscopic surgery [33,34]. Sentinel lymph node detection entails interstitial injection of a tracer, which results in a local high concentration of the tracer. However, there is a limited number of studies regarding commercially available laparoscopes for use with (tumour-targeted) IRDye800CW tracers [35,36]. Comparison of different systems is difficult as intraoperative detection of a fluorophore is dependent on various biological and optical factors [37]. Therefore, we conducted a systematic in vitro study with a NIRF calibration device. This phantom study aimed to explore the use of IRDye800CW, as an example conjugated to bevacizumab, with four commercially available NIRF laparoscopic surgical systems.

2. Materials and Methods

2.1. Phantom Set-Up

Clinical-grade bevacizumab-800CW was manufactured according to current Good Manufacturing Practice and supplied by the University Medical Center Groningen for use in this phantom study, as previously described [28]. In summary, bevacizumab (Roche Holding AG, Basel, Switzerland) and IRDye-800CW-NHS (LI-COR Biosciences, Lincoln, NE, USA) were conjugated with a dye to antibody ratio of 1.6:1 and formulated in a sodium chloride solution. Fifteen concentrations were created using serial dilution, starting from the standard concentration 6.8 μM (1 mg/mL bevacizumab-800CW), using 1:1 dilution with PBS, ending at 0.42 nM.

ICG (Verdye, Diagnostic Green GmbH, Aschheim-Dornach, Germany) was used as a fluorescent reference for bevacizumab-800CW. ICG was combined with 2% intralipid and PBS. Intralipid acted as human albumin in blood serum and was required for this phantom study, as ICG dissolved in water for injection or PBS has a different excitation and emission wavelength [38]. The ICG solution was serially diluted from the manufacture's recommended dose (5 mg/mL = 6.5 mM), similar to bevacizumab-800CW, resulting in the lowest concentration of 0.39 μM.

The molar concentration of ICG serial dilutions were a factor 950 higher than the bevacizumab-800CW concentrations, and 597 times higher than the molar concentration IRDye800CW due to the 1.6:1 dye to antibody ratio. Therefore, the first five concentrations of bevacizumab-800CW serial dilutions correspond approximately to the last five concentrations of ICG (Appendix A Table A1).

Transparent polypropylene Eppendorf tubes were filled with the solutions of bevacizumab-800CW or ICG and placed in a CalibrationDisk (SurgVision, Munich, Germany) [37,39]. The CalibrationDisk is a calibration device for NIRF systems and can hold up to eight Eppendorf tubes (Figure 1a). Two windows in the calibration device, approximately the size of lymph nodes, allowed fluorescent intensity measurement for each tube. Fat tissue-mimicking hydrogel made from gelatine (2.5 g), agar (2.5 g), and water (200 mL) to recreate fat in the mesocolon, were used to cover the CalibrationDisk. Formulation of the hydrogel was adopted from a previous ICG assessment study [40]. A black box was used to limit the influence of ambient light and therefore create a comparable situation to in vivo use of laparoscopes.

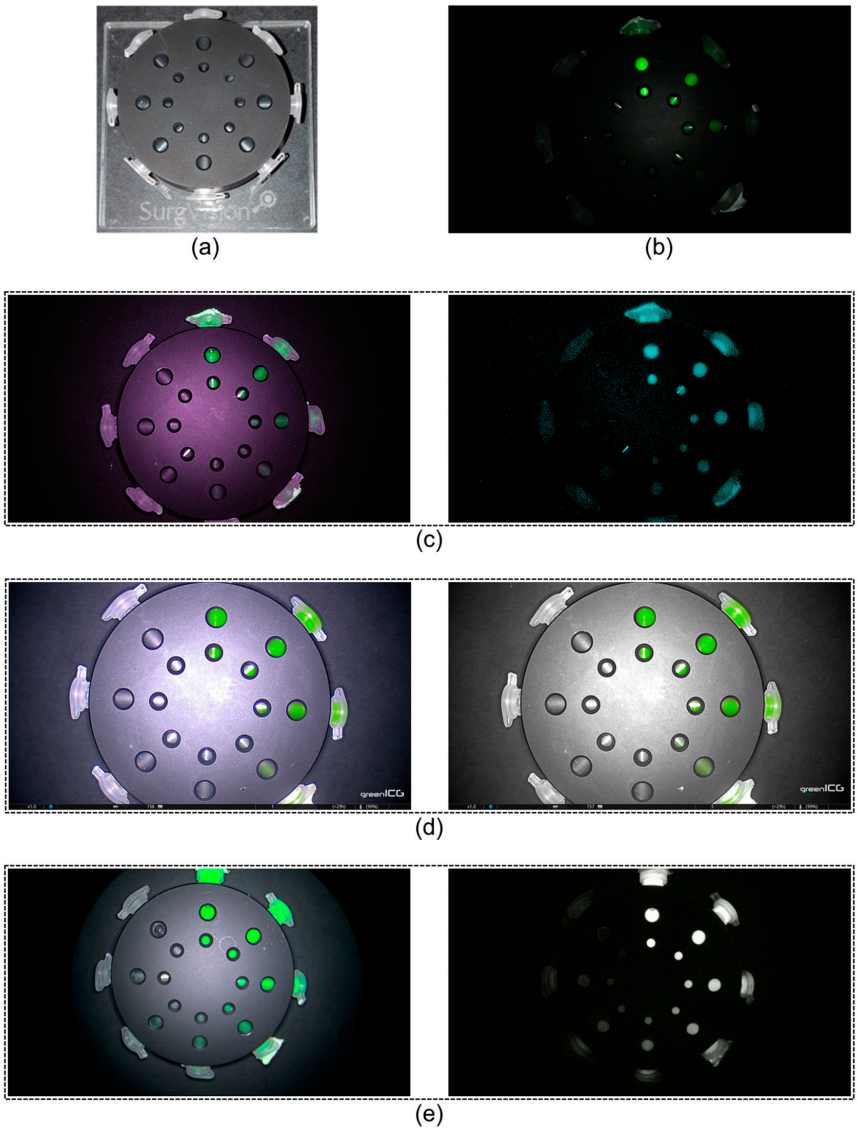


Figure 1. CalibrationDisk and near-infrared fluorescence modes of laparoscopes. (**a**) The CalibrationDisk for near-infrared fluorescence calibration with eight transparent Eppendorf tubes, and (**b**–**e**) serially diluted bevacizumab-800CW visible with four laparoscopes. (**b**) The da Vinci Xi had a single, monochromatic, fluorescence mode. (**c**) The VISERA ELITE II, (**d**) Rubina, and (**e**) ENDOCAM had a white light with fluorescence overlay mode (left column) in addition to a monochromatic mode (right column). The Rubina has a third mode, intensity map, that is not displayed since it was not tested in this study. The fluorescent light emitted by the fluorescent dyes were displayed as (a false) green or blue colour and superimposed over the images, except for the Rubina monochromatic image which was a true monochromatic mode. The pictures were all acquired at the same working distance (10.4 cm), therefore, differences in field of views depend on system properties.

2.2. Laparoscopic Near-Infrared Fluorescence Systems

Four commercially available laparoscopic systems for clinical use were tested: (1) VISERA ELITE II, Olympus; (2) ENDOCAM Logic 4K platform (short: ENDOCAM), Richard Wolf; (3) IMAGE1 S™ 4U Rubina (short: Rubina), KARL STORZ; and (4) da Vinci Xi, Intuitive Surgical (Figure 1). The VISERA ELITE II has a xenon lamp and the da Vinci Xi a laser source for NIRF excitation, while the other two systems use light emitting diodes (LEDs). Gain, software-based, to increase the fluorescence intensity, was automatically adjusted to improve visibility, except for the manually adjustable VISERA ELITE II system. Instead of gain, brightness of fluorescence could be manually changed for the ENDOCAM, Rubina, and da Vinci Xi to improve visibility. All systems have (at least) two fluorescence view mode options, except the da Vinci system with only one fluorescence view mode. Description of components, indications, and fields of use can be found in Appendix A Table A2.

2.3. Measurements

Imaging of phantoms, with different concentrations of bevacizumab-800CW and ICG, was performed with all four laparoscopic NIRF systems. Since 15 dilutions were used, imaging was performed in two steps by using the phantom of Figure 1a; the highest eight concentrations were imaged together in Eppendorf tubes, followed by the lowest seven concentrations. First, standard system settings (brightness, intensity or gain) were compared to high settings. High settings meant that the brightness, intensity or gain were maximised. Furthermore, imaging was performed in the different fluorescence modes when available. Next, working distance between laparoscope and phantom were varied to represent general working distances in laparoscopic surgery (8.7, 9.6 and 10.4 cm) while keeping all ROIs in the field of view. Last, visibility and tissue penetration were determined under optimal conditions per system. Up to three layers of tissue-mimicking hydrogels (0.8 cm in width each) were stacked to assess tissue penetration.

2.4. Data Analyses

The acquired fluorescence images were independently assessed for visibility by two researchers (DJS and AJS). Visibility of individual Eppendorf tubes was scored as visible or invisible and disagreement was resolved through discussion or a third researcher (ECJ). Consensus judgement of visibility was used for analyses since the interobserver agreement was almost perfect (kappa = 0.88) [41].

Segmentation of images was performed to evaluate the different image properties by three different parameters; target-to-background (or tumour-to-background, TBR; Equation (1)), signal-to-noise (SNR; Equation (2)), and contrast-to-noise (CNR; Equation (3)) ratio. The fluorescence signal was expressed in arbitrary units (AU). Regions of interest were defined as the windows in the CalibrationDisk (Appendix A Figure A1). TBR represents sensitivity to detect a fluorescent object from background and is frequently reported in clinical studies [16,23,42,43]. SNR is a measure comparing the signal, and therefore defines the sensitivity, and may be used to define the applicability of a tracer [43,44]. CNR is a measure based on contrast instead of the raw signal [44,45] Noise from background may influence detectability, thus CNR may be more representative in an environment with noise. System settings and working distance with the highest visibility were selected to assess the lowest visible concentration and tissue penetration depth. Analyses were performed with Matlab (2022b, The MathWorks, Portola Valley, CA, USA). No comparative tests were performed since this study explored the use of laparoscopes with bevacizumab-800CW instead of directly comparing equipment. Furthermore, photobleaching of IRDye800CW and ICG during measurements would lead to unfair comparison of laparoscopes [46–51].

$$\text{TBR} = \text{mean signal of ROI} / \text{mean signal of background} \quad (1)$$

$$\text{SNR} = \text{mean signal of ROI}/\text{standard deviation of signal in non-ROI (background)} \quad (2)$$

$$\text{CNR} = (\text{mean signal of ROI} - \text{mean signal in non-ROI (background)})/\text{standard deviation of signal in non-ROI (background)} \quad (3)$$

3. Results

3.1. Influence of System Settings and NIRF Mode on Visibility

Serial dilutions of bevacizumab-800CW (concentrations ranging from 0.42 to 6800 nM) and ICG (concentrations ranging from 394 nM to 6460 µM) were used to assessed visibility with different system settings and NIRF modes, totalling fourteen different scenarios with four laparoscopes for each fluorophore. Adjustment of brightness did not improve visibility of bevacizumab-800CW and ICG for the da Vinci Xi and ENDOCAM (Figure 2). All concentrations of bevacizumab-800CW were invisible with the standard settings of the VISERA ELITE II, independent from NIRF mode, while many of the ICG concentrations were visible with the same setting. However, bevacizumab-800CW was visible after the VISERA ELITE II system settings were manually adjusted. Likewise, adjusting fluorescence intensity led to visibility of lower concentrations when using the Rubina. Changing the fluorescence mode to a monochromatic view led to improvement in visibility of fluorophores for the VISERA ELITE II and Rubina, but it did not improve visibility of bevacizumab-800CW or ICG for the ENDOCAM. High system settings and monochromatic view often showed improved visibility and outcomes analysis.

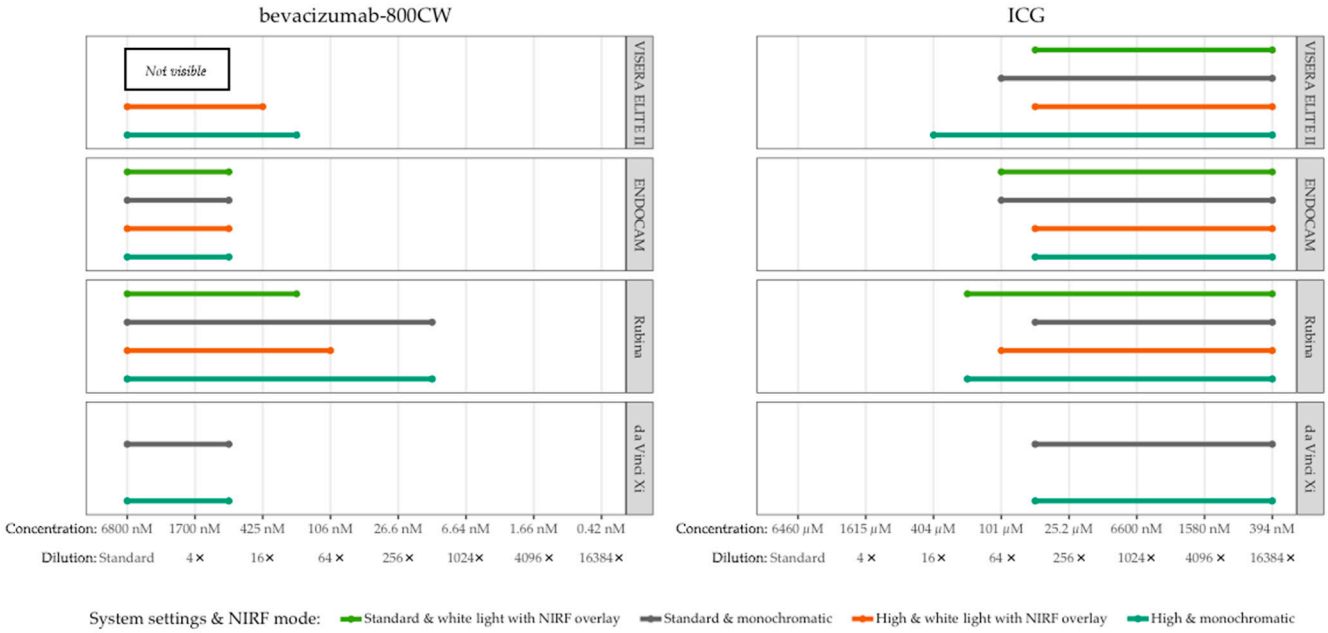


Figure 2. Visible concentrations of bevacizumab-800CW and ICG with four laparoscopes using varying system settings and NIRF modes. Adjusting system settings and switching to a monochromatic NIRF mode generally improved visibility of fluorophores for the VISERA ELITE II and Rubina. For example, bevacizumab-800CW was not visible with the standard settings of the VISERA ELITE II while it was visible with high system settings. Note(s): the da Vinci Xi does not have a white light with NIRF overlay mode.

3.2. Influence of Working Distance on Visibility

High camera settings and monochromatic NIRF mode were used to assess the influence of working distance to the phantom (Figure 3). In general, lower concentrations of bevacizumab-800CW were visible with the Rubina and VISERA ELITE II after the working distance was reduced to 8.7 cm. However, working distance did not influence visibility of bevacizumab-800CW and ICG for the ENDOCAM and da Vinci Xi. The smallest working distance, 8.7 cm, was used for assessment of visibility of concentrations and tissue penetration of the fluorescent signal.

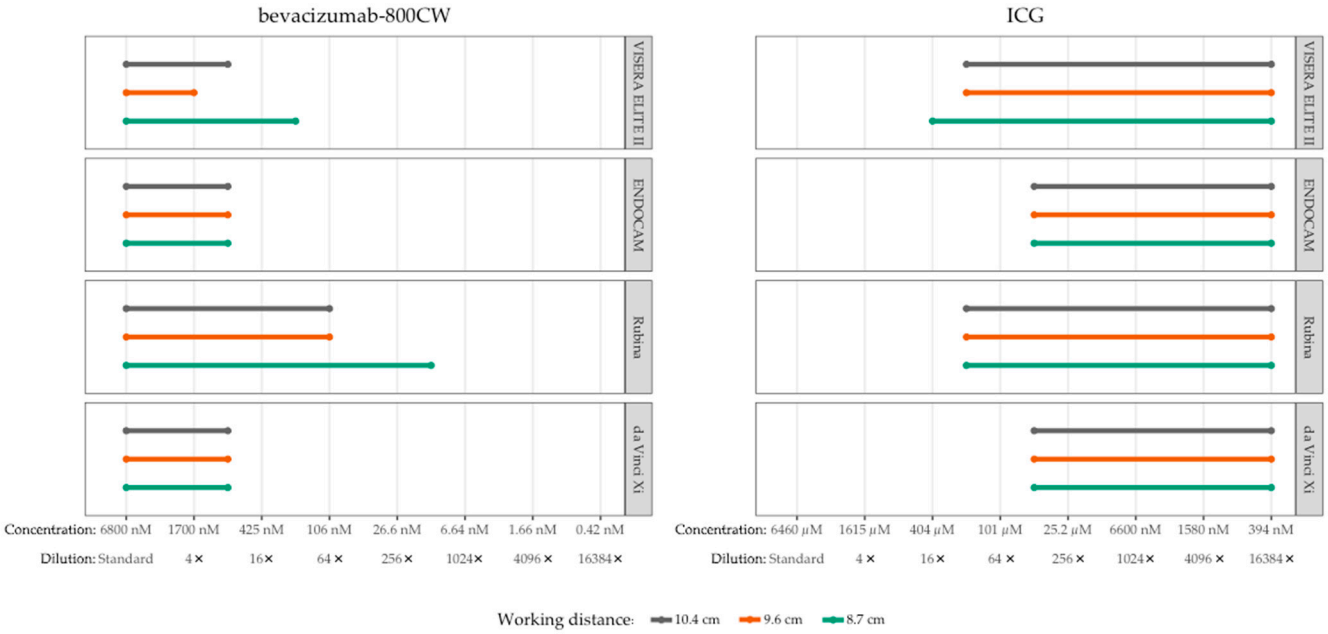


Figure 3. Visible concentrations of bevacizumab-800CW and ICG with four laparoscopes using varying working distances (8.7, 9.6 and 10.4 cm). Working distances were measured from tip of the laparoscope to the phantom. More concentrations of fluorophores were visible with reduced working distance using the VISERA ELITE II and Rubina, in accordance with the inverse-square law. The working distance did not influence visibility for the ENDOCAM and da Vinci Xi. Note(s): measurements performed with high system settings and monochromatic NIRF mode.

3.3. Visibility of Bevacizumab-800CW

The lowest visible concentrations of bevacizumab-800CW for the da Vinci Xi, ENDOCAM, VISERA ELITE II, and Rubina system were 850, 850, 213 and 13 nM (corresponding to 8, 8, 32 and 512 times diluted stock), respectively. In Figure 4 this is shown in grey.

The TBR, SNR, and CNR of the lowest visible concentration bevacizumab-800CW were: (1) VISERA ELITE II 2.90, 1.94, 1.27; (2) ENDOCAM 0.86, 2.52, −0.41; (3) Rubina 1.75, 2.53, 1.08; (4) da Vinci Xi 1.44, 1.44, 0.44, respectively (Figure 4). Primarily for the ENDOCAM and da Vinci Xi, there were invisible concentrations that had comparable or higher ratios than the last visible concentration.

TBR, SNR, and CNR were higher for the visible ICG concentrations compared to the bevacizumab-800CW concentrations, especially for the Rubina and da Vinci Xi (Figure 5e–h). However, the lowest visible concentration of ICG was not found with the serial dilutions used in this set up as the lowest available concentration of ICG was still visible.

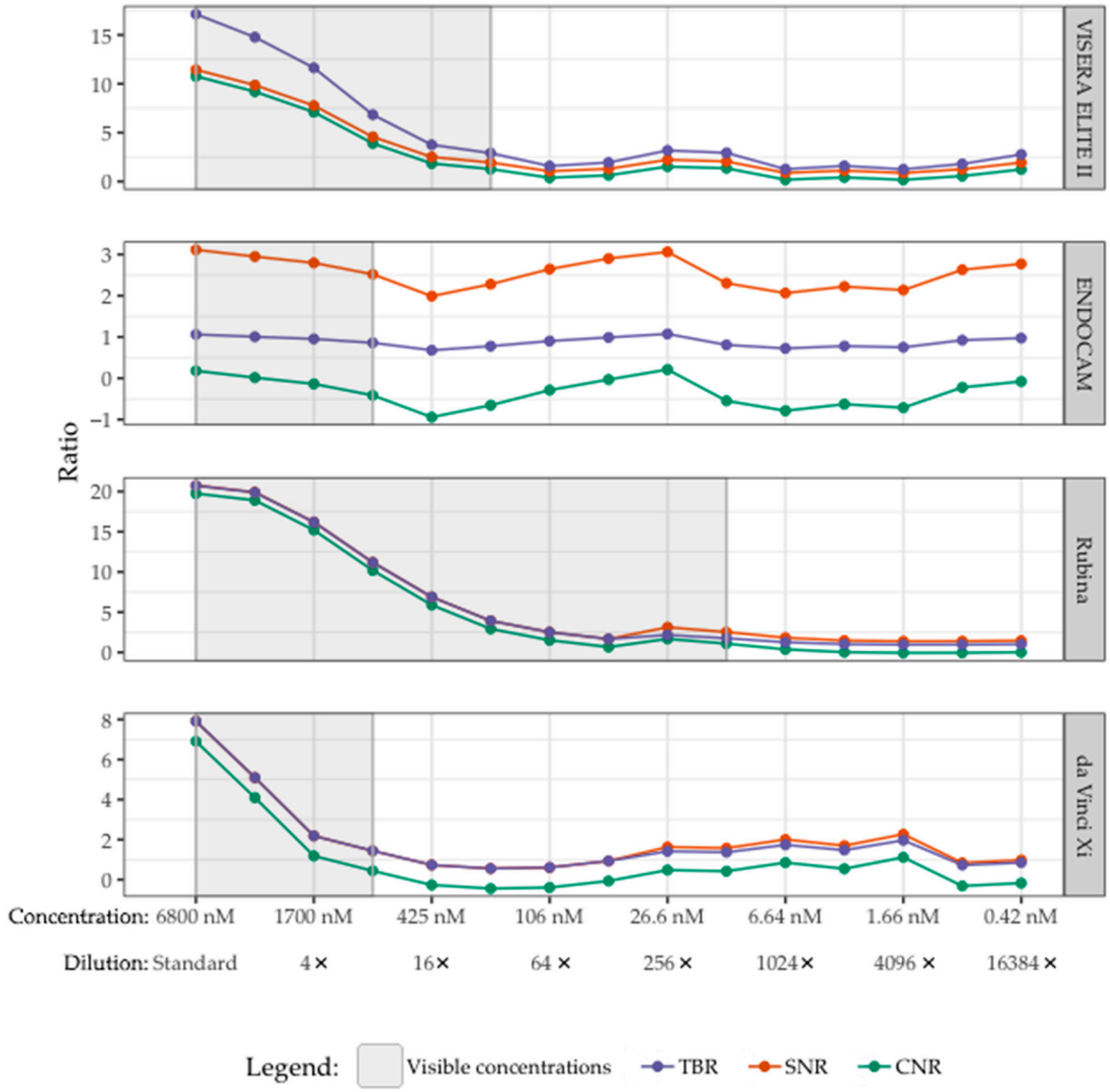


Figure 4. Visibility of bevacizumab-800CW with four laparoscopes correlated with TBR, SNR, and CNR. The visible concentrations per laparoscope are displayed in grey. The lowest visible concentrations of bevacizumab-800CW were 850, 850, 213 and 13 nM (corresponding to 8, 8, 32 and 512 times diluted stock) with the da Vinci Xi, ENDOCAM, VISERA ELITE II and Rubina, respectively. The TBR, SNR, and CNR decreased until bevacizumab-800CW was not visible anymore. However, there were higher TBRs/SNRs/CNRs for some invisible concentrations compared to the last visible concentration of bevacizumab-800CW, especially with the ENDOCAM and da Vinci Xi. Note(s): measurements performed with high system settings, monochromatic NIRF mode, and 8.7 cm working distance.

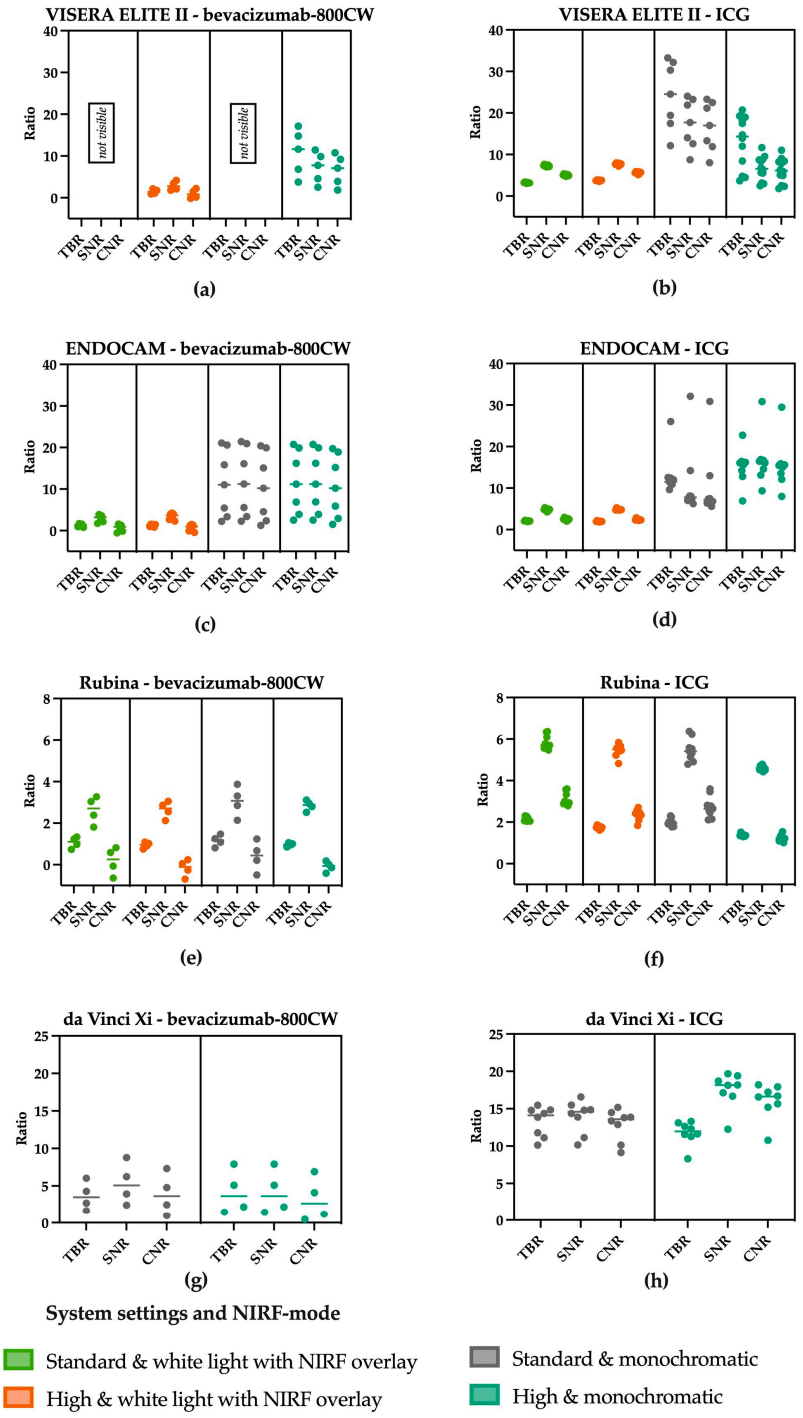


Figure 5. TBR, SNR and CNR of the visible concentration of bevacizumab-800CW and ICG using varying settings on laparoscopes. (**a**) bevacizumab-800CW using the VISERA ELITE II. (**b**) ICG using the VISERA ELITE II. A change in settings from standard to high increased the noise and therewith decreased the SNR and the CNR using the VISERA ELITE II. (**c**) bevacizumab-800CW using the ENDOCAM. (**d**) ICG using the ENDOCAM. Higher ratios were seen using the monochromatic view, suggesting better visibility using the ENDOCAM. (**e**) bevacizumab-800CW using the Rubina system. (**f**) ICG using the Rubina system. The Rubina barely showed changes in the ratios when changing the settings. (**g**) bevacizumab-800CW using the da Vinci Xi. (**h**) ICG using the da Vinci Xi. When increasing the system settings in the da Vinci Xi, a slight increase in the ratios was noted. Note: measurements performed with 8.7 cm working distance.

The ratios found using the VISERA ELITE II (Figure 5a,b) decrease when imaging ICG and the settings are changed from standard to high, especially for the SNR and CNR. Both are influenced by noise which increased with the use of higher settings. Switching to the monochromatic view of the ENDOCAM resulted in higher ratios compared to the white light fluorescence overlay mode (Figure 5c,d). In the Rubina system (Figure 5e,f) changing the system settings did not substantially change the ratios. Looking at the results using the da Vinci Xi (Figure 5g,h) it is striking to see that the SNR and CNR are higher when increasing the settings.

3.4. Tissue Penetration of Bevacizumab-800CW and ICG

Visibility of bevacizumab-800CW and ICG decreased with the amount of tissue-mimicking material (Figure 6). High concentrations (range 0.4–6.8 µM) of bevacizumab-800CW were visible in all systems with at least 0.8 cm of tissue-mimicking material, except for the da Vinci Xi. The Rubina and VISERA ELITE II were able to detect 1.7–6.8 µM bevacizumab-800CW through 1.6 cm of gel. In contrast, ICG could be detected through a minimum of 1.6 cm of tissue-mimicking material, and Rubina managed to detect ICG through 2.4 cm of gel. Interestingly, ICG concentration 9 with the VISERA ELITE II, and concentration 9 and 10 of the ENDOCAM were invisible using two gel layers while earlier and later concentrations were visible.

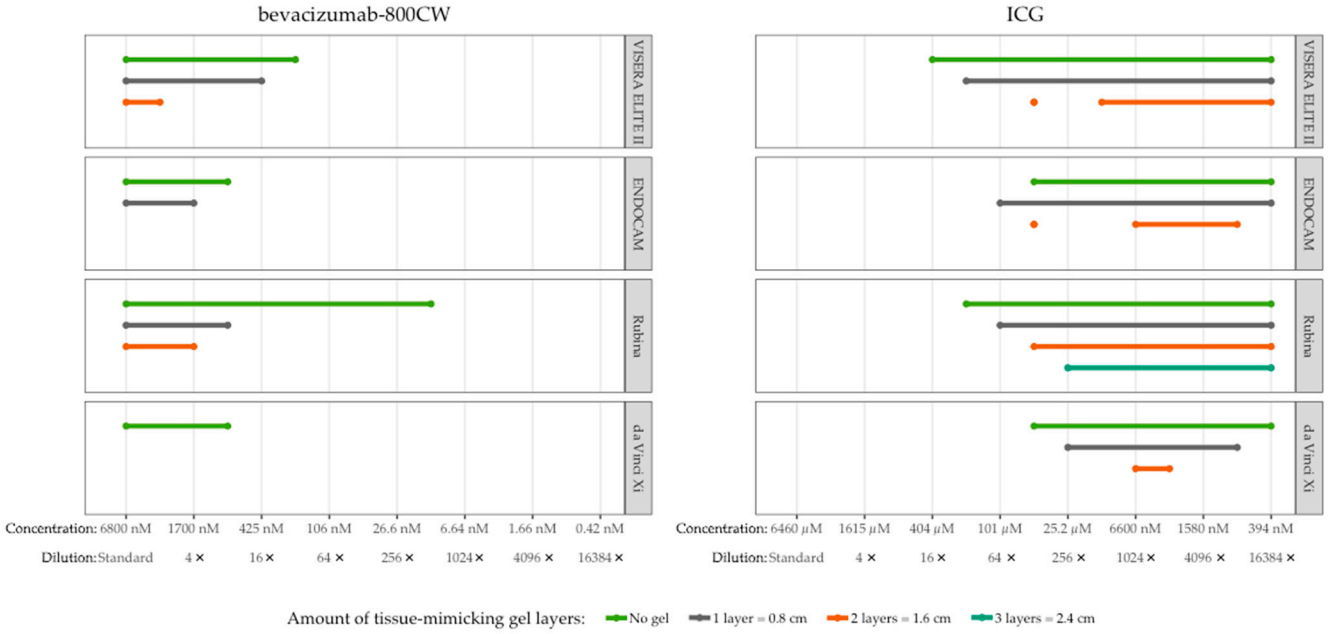


Figure 6. Tissue penetration of bevacizumab-800CW and ICG with four laparoscopes using tissue-mimicking gel. Bevacizumab-800CW was visible with all laparoscopes through 0.8 cm of gel, except for the da Vinci Xi (not visible through gel), and the Rubina was able to detect fluorescence through 1.6 cm of gel. By contrast, ICG could be detected through a minimum of 1.6 cm of gel, up to 2.4 cm with the Rubina. Note(s): measurements performed with high system settings, monochromatic NIRF mode, and 8.7 cm working distance.

4. Discussion

Image-guided surgery and NIRF could aid surgeons in intra-operative decision-making. This study explored the use of IRDye800CW, conjugated to bevacizumab, in vitro with four commercially available NIRF laparoscopic surgical systems intended for use with ICG. All four laparoscopes were able to detect bevacizumab-800CW in the highest concentrations, relevant for lymph node metastases detection after local administration, even though optimal absorption and emission wavelengths of IRDye800CW are different from ICG [13,38,52]. Depending on the system, bevacizumab-800CW could be detected

through up to 1.6 cm of tissue-mimicking material. In comparison, ICG was still visible after the standard solution was >16,000 times diluted and achieved 1.6–2.4 cm tissue penetration in all systems. In general, a surgeon could reduce the working distance and adjust system settings (gain, sensitivity or brightness) in order to improve visibility of bevacizumab-800CW.

In our study, laparoscopes were able to detect bevacizumab-800CW down to a concentration of 13–850 nM. In contrast, preclinical and clinical open-air camera systems, can detect ~0.05–15 nM bevacizumab-800CW in ideal conditions [14]. Visibility of bevacizumab-800CW with the laparoscopes might be sufficient for clinical use depending on the application, since an estimated 6–65,000 nM is required to detect ICG in sentinel lymph nodes after local injection [53] and IRDye800CW has a similar or higher quantum yield than ICG [54–56]. In an animal study, locally administered ^{99m}Tc-tilmanocept-800CW was successfully used for sentinel lymph node detection with a laparoscope [36]. Intravenously administered tumour-targeted tracers in micro-dosages will have a lower percentage of tracer uptake in metastatic lymph nodes; an estimated 0.3% of the injected dose [53]. In comparison, colonic adenomas contained an estimated 4.8–6.86 nM bevacizumab-800CW after 10–25 mg intravenous bevacizumab-800CW which should not be detectable with the laparoscopes [57]. Thus, the four laparoscopes might be insufficient to detect tumour-targeted bevacizumab-800CW in metastatic lymph nodes after intravenous injection or more tracer must be administered. Furthermore, promising results have already been achieved with tumour-targeted IRDye800CW for the detection of metastatic lymph nodes with open camera systems [58,59].

There is a wide range of conditions that influence visibility of tracers. For example, reduced working distance improved visibility in our study like it did in another study that assessed bevacizumab-800CW with an endoscope (Xenon light source with ICG filters and Image1S H3-Z FI camera from KARL STORZ) [60], due to the inverse-square law [61]. However, light reflections of tissue also increase with a decreased working distance and could give false information which may complicate decision making during surgery [60]. In the subjective assessment, ROIs were sometimes white instead of their intended NIRF green or blue colour (depending on the system) in the white light with overlay images. White ROIs were not considered to contain fluorescence, since white ROIs were due to light reflecting from tissue-mimicking gel or from oversaturation which may be caused due to high system settings. Therefore, some ICG concentrations were intermittently visible as seen in Figure 6 (VISERA ELITE II and ENDOCAM). Furthermore, ICG would only become visible after the stock was diluted >16 times. Invisibility of ICG in the highest concentrations is due to the aggregation of ICG molecules, which results in a substantial lower absorption wavelength (695 nm) [38] compared to the usual 800 nm absorption peak of ICG [13]. Quenching might also contribute to invisibility of ICG in >0.5 µg/mL concentrations [62] (roughly corresponding to 1024 times diluted stock in our study), but new research contradicts this claim [63].

In this phantom study, tissue penetration of bevacizumab-800CW and ICG was up to 1.6 cm and 1.6–2.4 cm through tissue-mimicking material, respectively. In earlier phantom studies, ICG could be detected through 3.6 mm of beeswax (optimal concentration after 200–2500 times diluted) [64], 6 mm of prostate-mimicking phantom (optimal concentration after 2000 times diluted) [65], and 2 cm of breast tissue-mimicking material [40]. Thus, fluorescence penetration varies in different tissues or phantoms due to optical properties, in addition to working distance and imaging properties [14]. Human or animal mesocolon could have been used for in vitro recreation of colon cancer sentinel lymph node detection. However, problems arose with the use of pig mesocolon as the tissue was heterogeneous and had an unstable shape, which hinders testing multiple surgical systems over multiple hours. The tissue-mimicking material used in this phantom study was homogenous and had similar optical absorption properties to human fat, thus allowing optimal comparison of multiple systems with the use of a calibration device [40]. Radioactive tracers are capable of achieving deeper tissue penetration compared to NIRF tracers. Utilisation of

hybrid radioactive and NIRF targeted tracers, such as ^{99m}Tc-tilmanocept-800CW [36] and ^{99m}Tc-ICG [66–68], would enable surgeons to benefit from the deeper tissue penetration of radioactive tracers for targeting lesions located further away while also allowing for more precise localisation of lesions in close range using NIRF. Future incorporation of augmented reality based on preoperative imaging presents another potential application for these hybrid tracers [69].

The lowest visible concentrations bevacizumab-800CW had a TBR ranging from 0.86 to 2.90, a SNR of 1.44 to 2.53, and a CNR of −0.41 to 1.27. Literature suggests that a TBR > 1.5 might be sufficient to discriminate fluorescent lesions and reduce false negatives in ideal situations. However, often a TBR > 2 is pursued for fluorescence-guided surgery and decision-making, and the TBR is also dependent on where it is measured [70]. For example, in vivo TBR would probably result in lower TBRs compared to ex vivo or in vitro measurements [70]. CNR might be more representative in an environment with noise and a CNR < 0 means less signal than noise, meaning that the ROI is not distinguishable from the background noise [44]. However, clear cut-off values for the ratios are not defined in the literature. Although visibility is a subjective parameter, this study showed a near-perfect interobserver agreement and its subsequent clinical applicability. Furthermore, objective image quality (described by SNR and CNR) did not always correspond to the subjective clinical visibility score. Some of the lowest visible concentrations were judged as visible but had a CNR < 0 and a TBR < 1. This could be due to multiple reasons. First, in the lowest visible samples the fluorescence signal was scarcely visible within the ROI, while the larger part of the remaining ROI was dark. This reduces the mean value of the ROI compared to the background leading to a negative CNR and low TBR. Second, the conversion of colour images to a grey scale, for segmentation purposes, may have decreased contrast. Two images, one acquired in monochromatic mode and one in coloured NIRF overlay mode, would result in different TBR/SNR/CNR after this segmentation process, but would have identical (subjective) visibility. Last, disagreement between objective and subjective assessment was seen in invisible concentrations that had a higher TBR/SNR/CNR than the last visible concentration, predominantly occurring with the ENDOCAM and da Vinci Xi. This might be explained by the automatic gain that is automatically applied to dark images in which no (or very little) fluorescence is detected. Often the second set of bevacizumab-800CW serial dilutions (with the lowest seven concentrations) in the phantom were predominantly invisible. Therefore, the second set of images were darker compared to first set of eight concentrations and more automatic gain would be applied.

Strengths and Limitations

To our knowledge, this is the first study looking into the use of commercially available laparoscopes of key market players and the use of a tumour-targeted tracer without modification of hardware or software. For this study, IRDye800CW conjugated to only bevacizumab was used as a tumour-targeted tracer. However, we hypothesise that other antibodies conjugated to IRDye800CW will have similar results, since the same NHS ester group is used for conjugation. Furthermore, absorption and emission wavelengths of IRDye800CW and hybrid targeted IRDye800CW tracers (e.g., ^{111}In-DTPA-trastuzumab-800CW and ^{68}Ga-tilmanocept-800CW) were comparable [71,72], unlike free ICG and ICG bound to albumin [38]. However, antibody-bound IRDye800CW or other tumour-targeted tracers are currently not yet approved by the FDA or EMA for application in general surgery. Nevertheless, the market for fluorescence-guided surgery is growing which might stimulate development of laparoscopic NIRF systems for tumour-targeted tracers [14]. A high sensitivity of laparoscopic NIRF systems for a tracer is one of the six key features described by Dsouza et al. and is especially important for tracers in micro-dosages [14]. However, micro-dosages of tumour-targeted bevacizumab-800CW have already been used for a broad range of indications with (experimental) open-air and endoscopic systems [18,19,21,24,57,59,73–76]. Thus, translation to optimised laparoscopes

should be achievable. In addition, the intended use for the laparoscopes, except the Olympus (Appendix A Table A2), already allows the use of fluorescence imaging for other fluorophores than ICG (e.g., IRDye800CW).

The different dilutions used, were too many to image all at once using the CalibrationDisk. Therefore, the highest eight concentrations and the lowest seven concentrations were imaged separately. This may have resulted in an unexpected intensity increase or decrease at the middle dilutions due to automatic adjustment of the images by some of the systems as also earlier described to cause an objective and subjective disagreement. Ideally a control dilution, used in both images, should have been used or all the used dilutions should have fitted in the CalibrationDisk.

Furthermore, the Rubina and da Vinci Xi laparoscopes had 30° optics while the other two laparoscopes were 0°. Ideally, only 0° optics would have been used, but the Rubina and da Vinci Xi 0° optics were unavailable at the time of the experiments. Measurements of the Rubina and da Vinci Xi were not postponed to keep all other variables constant. Nonetheless, the central viewing axis and working distances were kept constant between the different degree optics as these variables influence fluorescence intensity [64]. Furthermore, we do not expect the degrees of the optics to influence results as evident from a prior study [60]. However, we did not control for photobleaching of bevacizumab-800CW and ICG as we used the same samples for every laparoscope. Fluorescence intensity can halve after 30 min of near-infrared exposure [49]. Therefore, no conclusions can be drawn about which laparoscope is most sensitive to the fluorophores and future studies may want to control for photobleaching [40]. However, this study does suggest there are differences between usability of laparoscopes due to the wide range of the lowest visible concentration bevacizumab-800CW (13–850 nM). Consequently, surgeons should be aware that studies with fluorescent tracers (i.e., IRDye800CW and ICG) cannot directly be extrapolated to other laparoscopes or fluorescence imaging systems. Above all, each system has its own negative and positive properties and users should be aware of those properties when choosing a laparoscope for fluorescence imaging. Until there is a clear standardisation protocol for fluorescence imaging it will remain difficult to compare the sensitivity of different systems [77].

5. Conclusions

IRDye800CW, conjugated to bevacizumab, was visible with four commercially available laparoscopic surgical systems optimised for ICG with the lowest visible concentrations being 13–850 nM (equal to 8–512 times diluted stock). Tissue penetration of bevacizumab-800CW was up to 1.6 cm. In contrast, ICG was still visible after >16,000 times dilution and achieved tissue-penetration up to 2.4 cm. Depending on the application, visibility of bevacizumab-800CW might be sufficient for clinical use with current NIRF laparoscopes, but optimisation of sensitivity for IRDye800CW would widen the indication of tumour-targeted tracers in laparoscopic surgery. More future studies should focus on standardised testing of laparoscopes and their capabilities for detecting (new) NIRF tracers.

Author Contributions: Conceptualization, D.J.S., A.J.S., I.S., D.G., W.B.N. and E.C.J.C.; methodology, D.J.S., A.J.S., I.S., D.G., W.B.N. and E.C.J.C.; software, A.J.S., I.S. and D.G.; validation, D.J.S., A.J.S., W.B.N. and E.C.J.C.; formal analysis, D.J.S. and A.J.S.; investigation, D.J.S. and A.J.S.; resources, D.J.S., A.J.S. and E.C.J.C.; data curation, D.J.S. and A.J.S.; writing—original draft preparation, D.J.S. and A.J.S.; writing—review and editing, D.J.S., A.J.S., I.S., D.G., W.B.N. and E.C.J.C.; visualization, D.J.S., A.J.S., I.S., D.G., W.B.N. and E.C.J.C.; supervision, D.G., W.B.N. and E.C.J.C.; project administration, D.J.S., A.J.S.; I.S., D.G., W.B.N. and E.C.J.C.; funding acquisition, Not applicable. All authors have read and agreed to the published version of the manuscript.

Funding: This research received no external funding.

Institutional Review Board Statement: Not applicable.

Informed Consent Statement: Not applicable.

Data Availability Statement: The data presented in this study are available on reasonable request from the corresponding author.

Acknowledgments: The VISERA ELITE II, ENDOCAM, and Rubina laparoscopes were available for a try-and-buy trial period, while the da Vinci Xi was already available in the Meander Medical Centre. Therefore, we could conduct this phantom study with multiple laparoscopes. We would like to thank Tim Laagland (Olympus), Lennart Zijl (Arsis Medical B.V.; supplier of Richard Wolf), and Patrick Juch (Stöpler Medical B.V.; supplier of KARL STORZ) for their instructions of the laparoscopes. The acknowledged persons did not influence study design, data acquisition, statistical analyses, or interpretation of results. No right of review of the manuscript was requested or provided.

Conflicts of Interest: E.C.J.C. is proctor for Intuitive Surgical. No funding was obtained for this study. The suppliers of the laparoscopes had no role in the design of the study; in the collection, analyses, or interpretation of data; in the writing of the manuscript; or in the decision to publish the results.

Appendix A

Table A1. Concentration and dilution of two fluorophores: bevacizumab-800CW and ICG.

Sample	Dilution from the Standard Stock	Bevacizumab-800CW		ICG	
		mg/mL	Molar Concentration (M)	mg/mL	Molar Concentration (M)
1	Standard	1.00	6.80×10^{-3}	5.00	6.46
2	2	0.50	3.40×10^{-3}	2.50	3.23
3	4	0.25	1.70×10^{-3}	1.25	1.61
4	8	1.25×10^{-1}	8.50×10^{-4}	6.25×10^{-1}	8.07×10^{-1}
5	16	6.25×10^{-2}	4.25×10^{-4}	3.13×10^{-1}	4.04×10^{-1}
6	32	3.13×10^{-2}	2.13×10^{-4}	1.56×10^{-1}	2.02×10^{-1}
7	64	1.56×10^{-2}	1.06×10^{-4}	7.81×10^{-2}	1.01×10^{-1}
8	128	7.81×10^{-3}	5.31×10^{-5}	3.91×10^{-2}	5.05×10^{-2}
9	256	3.91×10^{-3}	2.66×10^{-5}	1.95×10^{-2}	2.52×10^{-2}
10	512	1.95×10^{-3}	1.33×10^{-5}	9.77×10^{-3}	1.26×10^{-2}
11	1024	9.77×10^{-4}	6.64×10^{-6}	4.88×10^{-3}	6.31×10^{-3}
12	2048	4.88×10^{-4}	3.32×10^{-6}	2.44×10^{-3}	3.15×10^{-3}
13	4096	2.44×10^{-4}	1.66×10^{-6}	1.22×10^{-3}	1.58×10^{-3}
14	8192	1.22×10^{-4}	8.30×10^{-7}	6.10×10^{-4}	7.89×10^{-4}
15	16,384	6.10×10^{-5}	4.15×10^{-7}	3.05×10^{-4}	3.94×10^{-4}

The standard stock solutions of bevacizumab-800CW and ICG were 1:1 serially diluted until the last sample was diluted 16,384 times. The molar concentration of the ICG stock is 950 times higher than the molar concentration of the bevacizumab-800CW stock. Therefore, the molar concentration of the first five samples of bevacizumab-800CW correspond approximately with the last five samples of ICG (highlighted in grey).

Table A2. Description of laparoscopic near-infrared fluorescence systems, system components, and indication for use of fluorescence.

Laparoscope Manufacturer	**VISERA ELITE II Olympus**	**ENDOCAM Logic 4k Richard Wolf**	**IMAGE1 S™ 4U Rubina KARL STORZ**	**da Vinci XiIntuitive Surgical**
Short name	VISERA ELITE II	ENDOCAM	Rubina	da Vinci Xi
NIRF excitation source, power	Xenon, 300W [78]	LED, 15W	LED, undisclosed	Laser, undisclosed
Excitation wavelength	Undisclosed	760–810 nm	Undisclosed	802–805 nm [79]
NIRF emission filter	Undisclosed	Undisclosed	Undisclosed	Undisclosed
System settings	No automatic gain. Manual intensity control	Automatic gain. Manual brightness control.	No automatic gain. Intensity manually adjustable	Automatic gain. Manual brightness control.
Fluorescence view mode(s)	1. "Standard mode": White light with green overlay 2. "Infrared enhancement mode": Monochromatic with blue overlay (6 field)	1. "greenICG mode": White light with green overlay 2. "greenICG pure mode":Monochromatic with green overlay	1. White light with green/blue overlay 2. Monochromatic 3. Intensity map (not used in this study)	1. "Firefly": Monochromatic with green overlay
System components				
Camera head	OLYMPUS CH-S200-XZ-EA (N5766550)	LOGIC HD CAMERA HEAD GREEN (85525812)	IMAGE1 S 4U Rubina, Opal1 NIR/ICG camera head (TH121)	Standard da Vinci Xi set-up (not the Endoscope Plus)
Light source	CLV-S200-IR (N5427050)	Light source LED green ENDOLIGHT (5165002)	Power LED RUBINA, OPAL1 NIR/ICG (TL400)	
Optic	WAIR100A (W8IR100A)	TELESCOPES 0° Ø 10 MM (8934461)	TIPCAM1 RUBINA (26003BRA)	
Video processor	OLYMPUS OTV-S200 (N5426850)	LOGIC 4K CAMERA CONTROLLER (5525301)	IMAGE1 S CONNECT II (TC201EN)	
Cable	WA03310A (WA03310A)	FIBER LIGHT CABLE Ø 5 MM (806550231)	Fiber Optic Light Cable, 300 cm, 4.8 mm (495TIP)	
Other	Not applicable	Not applicable	IMAGE1 S 4U-LINK (TC304)	

Table A2. *Cont.*

Laparoscope Manufacturer	VISERA ELITE II Olympus	ENDOCAM Logic 4k Richard Wolf	IMAGE1 S™ 4U Rubina KARL STORZ	da Vinci XiIntuitive Surgical
Indications and field of use for fluorescence	**Indication** An IR telescope is designed for fluorescence imaging in the near infrared range using indocyanine green (ICG) as dye. A filterexclusively designed for ICG is built into the telescope. Light of suitable wavelength passes through the filter and enhances visualization on compatible imaging systems.	**Indication** The products are used for the following indications in various medical disciplines: • Endoscopic operations • Visualization of the visceral blood flow • Lymph Node Mapping The products are used for fluorescence cholangiography, especially in laparoscopy. **Contra-indication** For fluorescence endoscopy (this relates to the indications of visceral blood flow, lymph node mapping and fluorescence cholangiography) please follow the specifications of the fluorescence dye manufacturer.	**Indication** NIR/ICG fluorescent light sources are intended for generating light in endoscopic and microscopic diagnostic examinations and in surgical procedures. **Intended use** For fluorescence endoscopy (this relates to the indications of visceral blood flow, lymph node mapping and fluorescence cholangiography) please follow the specifications of the fluorescence dye manufacturer. **Contra-indication** For fluorescence endoscopy (this relates to the indications of visceral blood flow, lymph node mapping and fluorescence cholangiography) please follow the specifications of the fluorescence dye manufacturer.	**Indications for use** [79] Upon intravenous administration and use of an ICG drug product consistent with its approved label, the da Vinci Fluorescence Imaging Vision System and the da Vinci Firefly Imaging System are intended to provide real-time endoscopic visible and near-infrared fluorescence imaging. The da Vinci Fluorescence Imaging Vision System and the da Vinci Firefly Imaging System enable surgeons to perform minimally invasive surgery using standard endoscopic visible light as well as visual assessment of vessels, blood flow and related tissue perfusion, and at least one of the major extrahepatic bile ducts (cystic duct, common bile duct or common hepatic duct), using near infrared imaging. Fluorescence imaging of biliary ducts with the da Vinci Fluorescence Imaging Vision System and da Vinci Firefly Imaging System are intended for use with standard of care white light and, when indicated, intraoperative cholangiography. The device is not intended for standalone use for biliary duct visualization.

Table A2. *Cont.*

Laparoscope Manufacturer	VISERA ELITE II Olympus	ENDOCAM Logic 4k Richard Wolf	IMAGE1 S™ 4U Rubina KARL STORZ	da Vinci XiIntuitive Surgical
				Upon interstitial administration and use of an ICG drug product consistent with its approved label, the da Vinci Fluorescence Imaging Vision System and the da Vinci Firefly Imaging System is used to perform intraoperative fluorescence imaging and visualization of the lymphatic system, including lymphatic vessels and lymph nodes.



Figure A1. CalibrationDisk with regions of interest and background highlighted. The CalibrationDisk for near-infrared fluorescence calibration with eight transparent Eppendorf tubes. Regions of interest (ROIs), defined as the windows in the CalibrationDisk of one sample, are displayed in green. Background was defined as the surface of the CalibrationDisk around the ROIs, displayed in red. The caps of Eppendorf tubes could show fluorescence, however, this was not considered as visible or an ROI. ROIs and background were used to calculate target-to-background (TBR), signal-to-noise (SNR), and contrast-to-noise (CNR).

References

1. Galema, H.A.; Meijer, R.P.J.; Lauwerends, L.J.; Verhoef, C.; Burggraaf, J.; Vahrmeijer, A.L.; Hutteman, M.; Keereweer, S.; Hilling, D.E. Fluorescence-Guided Surgery in Colorectal Cancer; A Review on Clinical Results and Future Perspectives. *Eur. J. Surg. Oncol. J. Eur. Soc. Surg. Oncol. Br. Assoc. Surg. Oncol.* **2022**, *48*, 810–821. [CrossRef] [PubMed]
2. Li, C.; Chen, G.; Zhang, Y.; Wu, F.; Wang, Q. Advanced Fluorescence Imaging Technology in the Near-Infrared-II Window for Biomedical Applications. *J. Am. Chem. Soc.* **2020**, *142*, 14789–14804. [CrossRef]
3. Kosaka, N.; Ogawa, M.; Choyke, P.L.; Kobayashi, H. Clinical Implications of Near-Infrared Fluorescence Imaging in Cancer. *Future Oncol.* **2009**, *5*, 1501–1511. [CrossRef] [PubMed]
4. Young, J.K.; Figueroa, E.R.; Drezek, R.A. Tunable Nanostructures as Photothermal Theranostic Agents. *Ann. Biomed. Eng.* **2012**, *40*, 438–459. [CrossRef]
5. Bashkatov, A.N.; Genina, E.A.; Kochubey, V.I.; Tuchin, V.V. Optical Properties of Human Skin, Subcutaneous and Mucous Tissues in the Wavelength Range from 400 to 2000 Nm. *J. Phys. D Appl. Phys.* **2005**, *38*, 2543. [CrossRef]
6. Speich, R. Anaphylactoid Reactions after Indocyanine-Green Administration. *Ann. Intern. Med.* **1988**, *109*, 345. [CrossRef]
7. She, W.H.; Cheung, T.T.; Chan, M.Y.; Chu, K.W.; Ma, K.W.; Tsang, S.H.Y.; Dai, W.C.; Chan, A.C.Y.; Lo, C.M. Routine Use of ICG to Enhance Operative Safety in Emergency Laparoscopic Cholecystectomy: A Randomized Controlled Trial. *Surg. Endosc.* **2022**, *36*, 4442–4451. [CrossRef] [PubMed]
8. Schouw, H.M.; Huisman, L.A.; Janssen, Y.F.; Slart, R.H.J.A.; Borra, R.J.H.; Willemsen, A.T.M.; Brouwers, A.H.; van Dijl, J.M.; Dierckx, R.A.; van Dam, G.M.; et al. Targeted Optical Fluorescence Imaging: A Meta-Narrative Review and Future Perspectives. *Eur. J. Nucl. Med. Mol. Imaging* **2021**, *48*, 4272–4292. [CrossRef]
9. Harlaar, N.J.; Koller, M.; de Jongh, S.J.; van Leeuwen, B.L.; Hemmer, P.H.; Kruijff, S.; van Ginkel, R.J.; Been, L.B.; de Jong, J.S.; Kats-Ugurlu, G.; et al. Molecular Fluorescence-Guided Surgery of Peritoneal Carcinomatosis of Colorectal Origin: A Single-Centre Feasibility Study. *Lancet Gastroenterol. Hepatol.* **2016**, *1*, 283–290. [CrossRef]

10. Lwin, T.M.; Turner, M.A.; Amirfakhri, S.; Nishino, H.; Hoffman, R.M.; Bouvet, M. Fluorescence Molecular Targeting of Colon Cancer to Visualize the Invisible. *Cells* **2022**, *11*, 249. [CrossRef] [PubMed]
11. LI-COR Biosciences IRDye®Infrared Dyes. Available online: https://www.ld.ru/w/licor/IRDye_brochure_web.pdf (accessed on 8 January 2023).
12. AAT Bioquest Spectrum [Li-Cor IRDye 800CW]. Available online: https://www.aatbio.com/fluorescence-excitation-emission-spectrum-graph-viewer/li_cor_irdye_800cw (accessed on 8 January 2023).
13. Landsman, M.L.; Kwant, G.; Mook, G.A.; Zijlstra, W.G. Light-Absorbing Properties, Stability, and Spectral Stabilization of Indocyanine Green. *J. Appl. Physiol.* **1976**, *40*, 575–583. [CrossRef]
14. DSouza, A.V.; Lin, H.; Henderson, E.R.; Samkoe, K.S.; Pogue, B.W. Review of Fluorescence Guided Surgery Systems: Identification of Key Performance Capabilities beyond Indocyanine Green Imaging. *J. Biomed. Opt.* **2016**, *21*, 80901. [CrossRef] [PubMed]
15. Lamberts, L.; Koch, M.; de Jong, J.; Adams, A.; Glatz, J.; Kranendonk, M.; Terwisscha van Scheltinga, A.; Jansen, L.; de Vries, J.; Lub-de Hooge, M.; et al. Tumor-Specific Uptake of Fluorescent Bevacizumab-IRDye800CW Microdosing in Patients with Primary Breast Cancer: A Phase I Feasibility Study. *Clin Cancer Res.* **2017**, *23*, 2730–2741. [CrossRef] [PubMed]
16. Nagengast, W.B.; Hartmans, E.; Garcia-Allende, P.B.; Peters, F.T.M.; Linssen, M.D.; Koch, M.; Koller, M.; Tjalma, J.J.J.; Karrenbeld, A.; Jorritsma-Smit, A.; et al. Near-Infrared Fluorescence Molecular Endoscopy Detects Dysplastic Oesophageal Lesions Using Topical and Systemic Tracer of Vascular Endothelial Growth Factor A. *Gut* **2019**, *68*, 7–10. [CrossRef] [PubMed]
17. Tjalma, J.J.J.; Koller, M.; Linssen, M.D.; Hartmans, E.; de Jongh, S.J.; Jorritsma-Smit, A.; Karrenbeld, A.; de Vries, E.G.; Kleibeuker, J.H.; Pennings, J.P.; et al. Quantitative Fluorescence Endoscopy: An Innovative Endoscopy Approach to Evaluate Neoadjuvant Treatment Response in Locally Advanced Rectal Cancer. *Gut* **2020**, *69*, 406–410. [CrossRef] [PubMed]
18. Mulder, B.G.S.; Koller, M.; Duiker, E.W.; Sarasqueta, A.F.; Burggraaf, J.; de Meijer, V.E.; Vahrmeijer, A.L.; Hoogwater, F.J.H.; Bonsing, B.A.; van Dam, G.M.; et al. Intraoperative Molecular Fluorescence Imaging of Pancreatic Cancer by Targeting Vascular Endothelial Growth Factor: A Multicenter Feasibility Dose-Escalation Study. *J. Nucl. Med.* **2023**, *64*, 82–89. [CrossRef]
19. Vonk, J.; Voskuil, F.J.; de Wit, J.G.; Heeman, W.T.; Nagengast, W.B.; van Dam, G.M.; Feijen, R.A.; Korsten-Meijer, A.; van der Vegt, B.; Witjes, M. Fluorescence Grid Analysis for the Evaluation of Piecemeal Surgery in Sinonasal Inverted Papilloma: A Proof-of-Concept Study. *Eur. J. Nucl. Med. Mol. Imaging* **2022**, *49*, 1640–1649. [CrossRef] [PubMed]
20. Steinkamp, P.J.; Vonk, J.; Huisman, L.A.; Meersma, G.-J.; Diercks, G.F.H.; Hillebrands, J.-L.; Nagengast, W.B.; Zeebregts, C.J.; Slart, R.H.J.A.; Boersma, H.H.; et al. VEGF-Targeted Multispectral Optoacoustic Tomography and Fluorescence Molecular Imaging in Human Carotid Atherosclerotic Plaques. *Diagnostics* **2021**, *11*, 1227. [CrossRef]
21. Steinkamp, P.J.; Pranger, B.K.; Li, M.-F.; Linssen, M.D.; Voskuil, F.J.; Been, L.B.; van Leeuwen, B.L.; Suurmeijer, A.J.H.; Nagengast, W.B.; Kruijff, S.; et al. Fluorescence-Guided Visualization of Soft-Tissue Sarcomas by Targeting Vascular Endothelial Growth Factor A: A Phase 1 Single-Center Clinical Trial. *J. Nucl. Med.* **2021**, *62*, 342–347. [CrossRef]
22. De Jongh, S.J.; Tjalma, J.J.J.; Koller, M.; Linssen, M.D.; Vonk, J.; Dobosz, M.; Jorritsma-Smit, A.; Kleibeuker, J.H.; Hospers, G.A.P.; Havenga, K.; et al. Back-Table Fluorescence-Guided Imaging for Circumferential Resection Margin Evaluation Using Bevacizumab-800CW in Patients with Locally Advanced Rectal Cancer. *J. Nucl. Med.* **2020**, *61*, 655–661. [CrossRef]
23. Vonk, J.; de Wit, J.G.; Voskuil, F.J.; Koldijk, M.; Rácz, E.; Hooghiemstra, W.T.R.; Doff, J.J.; Diercks, G.F.H.; van Dam, G.M.; Witjes, M.J.H.; et al. Fluorescence Molecular Imaging Using Cetuximab-800CW in Cutaneous Squamous Cell Carcinoma Surgery: A Proof-of-Concept Study. *Br. J. Dermatol.* **2022**, *187*, 810–812. [CrossRef]
24. Vonk, J.; de Wit, J.G.; Voskuil, F.J.; Tang, Y.H.; Hooghiemstra, W.T.R.; Linssen, M.D.; van den Broek, E.; Doff, J.J.; de Visscher, S.A.H.J.; Schepman, K.-P.; et al. Epidermal Growth Factor Receptor-Targeted Fluorescence Molecular Imaging for Postoperative Lymph Node Assessment in Patients with Oral Cancer. *J. Nucl. Med.* **2022**, *63*, 672–678. [CrossRef] [PubMed]
25. Linssen, M.D.; Hooghiemstra, W.T.R.; Jorritsma-Smit, A.; Allersma, D.P.; Dijkstra, G.; Nagengast, W.B. Development and Characterisation of Antibody-Based Optical Imaging Probes for Inflammatory Bowel Disease. *Pharmaceuticals* **2021**, *14*, 922. [CrossRef]
26. Zhao, X.; Gabriëls, R.Y.; Hooghiemstra, W.T.R.; Koller, M.; Meersma, G.J.; Buist-Homan, M.; Visser, L.; Robinson, D.J.; Tenditnaya, A.; Gorpas, D.; et al. Validation of Novel Molecular Imaging Targets Identified by Functional Genomic MRNA Profiling to Detect Dysplasia in Barrett's Esophagus. *Cancers* **2022**, *14*, 2462. [CrossRef]
27. Linssen, M.D.; Ter Weele, E.J.; Allersma, D.P.; Lub-de Hooge, M.N.; van Dam, G.M.; Jorritsma-Smit, A.; Nagengast, W.B. Roadmap for the Development and Clinical Translation of Optical Tracers Cetuximab-800CW and Trastuzumab-800CW. *J. Nucl. Med.* **2019**, *60*, 418–423. [CrossRef]
28. Ter Weele, E.J.; Terwisscha van Scheltinga, A.G.T.; Linssen, M.D.; Nagengast, W.B.; Lindner, I.; Jorritsma-Smit, A.; de Vries, E.G.E.; Kosterink, J.G.W.; Lub-de Hooge, M.N. Development, Preclinical Safety, Formulation, and Stability of Clinical Grade Bevacizumab-800CW, a New near Infrared Fluorescent Imaging Agent for First in Human Use. *Eur. J. Pharm. Biopharm. Off. J. Arb. Pharm. Verfahr.* **2016**, *104*, 226–234. [CrossRef]
29. U.S. Department of Health and Human Services Food and Drug Administration Center for Drug. Evaluation and Research (CDER) Guidance for Industry, Investigators, and Reviewers—Exploratory IND Studies. Available online: https://www.fda.gov/media/72325/download (accessed on 2 March 2023).
30. European Medicines Agency (EMA). *ICH Guideline M3(R2) on Non-Clinical Safety Studies for the Conduct of Human Clinical Trials and Marketing Authorisation for Pharmaceuticals*; European Medicines Agency: Amsterdam, The Netherlands, 2013.
31. Tewari, T.; Mukherjee, S. Microdosing: Concept, Application and Relevance. *Perspect. Clin. Res.* **2010**, *1*, 61–63.

32. Burt, T.; Young, G.; Lee, W.; Kusuhara, H.; Langer, O.; Rowland, M.; Sugiyama, Y. Phase 0/Microdosing Approaches: Time for Mainstream Application in Drug Development? *Nat. Rev. Drug Discov.* **2020**, *19*, 801–818. [CrossRef] [PubMed]
33. Sikkenk, D.; Consten, E.; Nagengast, W. Clinicaltrials.Gov—Fluorescent Sentinel Lymph Node Identification in Colon Carcinoma Using Submucosal Bevacizumab-800CW. (IBIZA-1). Available online: https://clinicaltrials.gov/ct2/show/NCT05498051?term=bevacizumab-800CW&recrs=ab&cntry=NL&draw=2&rank=2 (accessed on 1 March 2023).
34. Sikkenk, D.; Nagengast, W.; Consten, E. Clinicaltrials.Gov—Fluorescent Sentinel Lymph Node Identification in Colon Carcinoma Using Intravenous Bevacizumab-800CW. (IBIZA-2). Available online: https://clinicaltrials.gov/ct2/show/NCT05497726?term=bevacizumab-800CW&recrs=ab&cntry=NL&draw=2&rank=1 (accessed on 1 March 2023).
35. Korb, M.L.; Huh, W.K.; Boone, J.D.; Warram, J.M.; Chung, T.K.; de Boer, E.; Bland, K.I.; Rosenthal, E.L. Laparoscopic Fluorescent Visualization of the Ureter With Intravenous IRDye800CW. *J. Minim. Invasive Gynecol.* **2015**, *22*, 799–806. [CrossRef]
36. Liss, M.A.; Farshchi-Heydari, S.; Qin, Z.; Hickey, S.A.; Hall, D.J.; Kane, C.J.; Vera, D.R. Preclinical Evaluation of Robotic-Assisted Sentinel Lymph Node Fluorescence Imaging. *J. Nucl. Med.* **2014**, *55*, 1552–1556. [CrossRef] [PubMed]
37. Hoogstins, C.; Burggraaf, J.J.; Koller, M.; Handgraaf, H.; Boogerd, L.; van Dam, G.; Vahrmeijer, A.; Burggraaf, J. Setting Standards for Reporting and Quantification in Fluorescence-Guided Surgery. *Mol. Imaging Biol.* **2019**, *21*, 11–18. [CrossRef]
38. Yuan, B.; Chen, N.; Zhu, Q. Emission and Absorption Properties of Indocyanine Green in Intralipid Solution. *J. Biomed. Opt.* **2004**, *9*, 497–503. [CrossRef] [PubMed]
39. Voskuil, F.J.; Steinkamp, P.J.; Zhao, T.; van der Vegt, B.; Koller, M.; Doff, J.J.; Jayalakshmi, Y.; Hartung, J.P.; Gao, J.; Sumer, B.D.; et al. Exploiting Metabolic Acidosis in Solid Cancers Using a Tumor-Agnostic PH-Activatable Nanoprobe for Fluorescence-Guided Surgery. *Nat. Commun.* **2020**, *11*, 3257. [CrossRef]
40. Pleijhuis, R.; Timmermans, A.; De Jong, J.; De Boer, E.; Ntziachristos, V.; Van Dam, G. Tissue-Simulating Phantoms for Assessing Potential near-Infrared Fluorescence Imaging Applications in Breast Cancer Surgery. *J. Vis. Exp.* **2014**, 51776. [CrossRef]
41. Viera, A.J.; Garrett, J.M. Understanding Interobserver Agreement: The Kappa Statistic. *Fam. Med.* **2005**, *37*, 360–363.
42. Koller, M.; Qiu, S.-Q.; Linssen, M.D.; Jansen, L.; Kelder, W.; de Vries, J.; Kruithof, I.; Zhang, G.-J.; Robinson, D.J.; Nagengast, W.B.; et al. Implementation and Benchmarking of a Novel Analytical Framework to Clinically Evaluate Tumor-Specific Fluorescent Tracers. *Nat. Commun.* **2018**, *9*, 3739. [CrossRef] [PubMed]
43. Garcia-Allende, P.; Glatz, J.; Koch, M.; Tjalma, J.; Hartmans, E.; Terwisscha van Scheltinga, A.; Symvoulidis, P.; van Dam, G.; Nagengast, W.; Ntziachristos, V. Towards Clinically Translatable NIR Fluorescence Molecular Guidance for Colonoscopy. *Biomed. Opt. Express* **2013**, *5*, 78–92. [CrossRef]
44. Welvaert, M.; Rosseel, Y. On the Definition of Signal-to-Noise Ratio and Contrast-to-Noise Ratio for FMRI Data. *PLoS ONE* **2013**, *8*, e77089. [CrossRef]
45. Song, X.; Pogue, B.W.; Jiang, S.; Doyley, M.M.; Dehghani, H.; Tosteson, T.D.; Paulsen, K.D. Automated Region Detection Based on the Contrast-to-Noise Ratio in near-Infrared Tomography. *Appl. Opt.* **2004**, *43*, 1053–1062. [CrossRef]
46. Dempsey, G.T.; Vaughan, J.C.; Chen, K.H.; Bates, M.; Zhuang, X. Evaluation of Fluorophores for Optimal Performance in Localization-Based Super-Resolution Imaging. *Nat. Methods* **2011**, *8*, 1027–1036. [CrossRef]
47. Te Velde, E.A.; Veerman, T.; Subramaniam, V.; Ruers, T. The Use of Fluorescent Dyes and Probes in Surgical Oncology. *Eur. J. Surg. Oncol. J. Eur. Soc. Surg. Oncol. Br. Assoc. Surg. Oncol.* **2010**, *36*, 6–15. [CrossRef]
48. Pang, Z.; Yan, W.; Yang, J.; Li, Q.; Guo, Y.; Zhou, D.; Jiang, X. Multifunctional Gold Nanoclusters for Effective Targeting, Near-Infrared Fluorescence Imaging, Diagnosis, and Treatment of Cancer Lymphatic Metastasis. *ACS Nano* **2022**, *16*, 16019–16037. [CrossRef]
49. Mok, H.; Jeong, H.; Kim, S.-J.; Chung, B.H. Indocyanine Green Encapsulated Nanogels for Hyaluronidase Activatable and Selective near Infrared Imaging of Tumors and Lymph Nodes. *Chem. Commun. (Camb).* **2012**, *48*, 8628–8630. [CrossRef]
50. Holzer, W.; Mauerer, M.; Penzkofer, A.; Szeimies, R.M.; Abels, C.; Landthaler, M.; Bäumler, W. Photostability and Thermal Stability of Indocyanine Green. *J. Photochem. Photobiol. B* **1998**, *47*, 155–164. [CrossRef] [PubMed]
51. Saxena, V.; Sadoqi, M.; Shao, J. Enhanced Photo-Stability, Thermal-Stability and Aqueous-Stability of Indocyanine Green in Polymeric Nanoparticulate Systems. *J. Photochem. Photobiol. B* **2004**, *74*, 29–38. [CrossRef]
52. Prahl, S. Optical Absorption of Indocyanine Green (ICG). Available online: https://omlc.org/spectra/icg/index.html (accessed on 8 January 2023).
53. KleinJan, G.H.; Bunschoten, A.; van den Berg, N.S.; Olmos, R.A.V.; Klop, W.M.C.; Horenblas, S.; van der Poel, H.G.; Wester, H.-J.; van Leeuwen, F.W.B. Fluorescence Guided Surgery and Tracer-Dose, Fact or Fiction? *Eur. J. Nucl. Med. Mol. Imaging* **2016**, *43*, 1857–1867. [CrossRef] [PubMed]
54. Carr, J.A.; Franke, D.; Caram, J.R.; Perkinson, C.F.; Saif, M.; Askoxylakis, V.; Datta, M.; Fukumura, D.; Jain, R.K.; Bawendi, M.G.; et al. Shortwave Infrared Fluorescence Imaging with the Clinically Approved Near-Infrared Dye Indocyanine Green. *Proc. Natl. Acad. Sci. USA* **2018**, *115*, 4465–4470. [CrossRef] [PubMed]
55. Heuveling, D.A.; Visser, G.W.M.; de Groot, M.; de Boer, J.F.; Baclayon, M.; Roos, W.H.; Wuite, G.J.L.; Leemans, C.R.; de Bree, R.; van Dongen, G.A.M.S. Nanocolloidal Albumin-IRDye 800CW: A near-Infrared Fluorescent Tracer with Optimal Retention in the Sentinel Lymph Node. *Eur. J. Nucl. Med. Mol. Imaging* **2012**, *39*, 1161–1168. [CrossRef]
56. Tanaka, E.; Choi, H.S.; Fujii, H.; Bawendi, M.G.; Frangioni, J.V. Image-Guided Oncologic Surgery Using Invisible Light: Completed Pre-Clinical Development for Sentinel Lymph Node Mapping. *Ann. Surg. Oncol.* **2006**, *13*, 1671–1681. [CrossRef]

57. Hartmans, E.; Tjalma, J.J.J.; Linssen, M.D.; Allende, P.B.G.; Koller, M.; Jorritsma-Smit, A.; Nery, M.E.S.d.O.; Elias, S.G.; Karrenbeld, A.; de Vries, E.G.E.; et al. Potential Red-Flag Identification of Colorectal Adenomas with Wide-Field Fluorescence Molecular Endoscopy. *Theranostics* **2018**, *8*, 1458–1467. [CrossRef] [PubMed]
58. Krishnan, G.; van den Berg, N.S.; Nishio, N.; Juniper, G.; Pei, J.; Zhou, Q.; Lu, G.; Lee, Y.-J.; Ramos, K.; Iagaru, A.H.; et al. Metastatic and Sentinel Lymph Node Mapping Using Intravenously Delivered Panitumumab-IRDye800CW. *Theranostics* **2021**, *11*, 7188–7198. [CrossRef]
59. Tummers, W.S.; Miller, S.E.; Teraphongphom, N.T.; van den Berg, N.S.; Hasan, A.; Longacre, T.A.; Fisher, G.A.; Bonsing, B.A.; Vahrmeijer, A.L.; Gambhir, S.S.; et al. Detection of Visually Occult Metastatic Lymph Nodes Using Molecularly Targeted Fluorescent Imaging during Surgical Resection of Pancreatic Cancer. *HPB Off. J. Int. Hepato Pancreato Biliary Assoc.* **2019**, *21*, 883–890. [CrossRef]
60. Hart, Z.P.; Nishio, N.; Krishnan, G.; Lu, G.; Zhou, Q.; Fakurnejad, S.; Wormald, P.J.; van den Berg, N.S.; Rosenthal, E.L.; Baik, F.M. Endoscopic Fluorescence-Guided Surgery for Sinonasal Cancer Using an Antibody-Dye Conjugate. *Laryngoscope* **2020**, *130*, 2811–2817. [CrossRef] [PubMed]
61. Bonfield, H.E.; Knauber, T.; Lévesque, F.; Moschetta, E.G.; Susanne, F.; Edwards, L.J. Photons as a 21st Century Reagent. *Nat. Commun.* **2020**, *11*, 804. [CrossRef] [PubMed]
62. Hollins, B.; Noe, B.; Henderson, J.M. Fluorometric Determination of Indocyanine Green in Plasma. *Clin. Chem.* **1987**, *33*, 765–768. [CrossRef] [PubMed]
63. Mindt, S.; Karampinis, I.; John, M.; Neumaier, M.; Nowak, K. Stability and Degradation of Indocyanine Green in Plasma, Aqueous Solution and Whole Blood. *Photochem. Photobiol. Sci. Off. J. Eur. Photochem. Assoc. Eur. Soc. Photobiol.* **2018**, *17*, 1189–1196. [CrossRef]
64. van den Bos, J.; Wieringa, F.P.; Bouvy, N.D.; Stassen, L.P.S. Optimizing the Image of Fluorescence Cholangiography Using ICG: A Systematic Review and Ex Vivo Experiments. *Surg. Endosc.* **2018**, *32*, 4820–4832. [CrossRef]
65. van Willigen, D.M.; van den Berg, N.S.; Buckle, T.; KleinJan, G.H.; Hardwick, J.C.; van der Poel, H.G.; van Leeuwen, F.W. Multispectral Fluorescence Guided Surgery; a Feasibility Study in a Phantom Using a Clinical-Grade Laparoscopic Camera System. *Am. J. Nucl. Med. Mol. Imaging* **2017**, *7*, 138–147.
66. Vreeburg, M.T.A.; Azargoshasb, S.; van Willigen, D.; Molenaar, T.; van Oosterom, M.N.; Buckle, T.; Slof, L.J.; Klop, M.; Karakullukcu, B.; Donswijk, M.; et al. Comparison of Two Hybrid Sentinel Node Tracers: Indocyanine Green (ICG)-(99m)Tc-Nanocolloid vs. ICG-(99m)Tc-Nanoscan from a Nuclear Medicine and Surgical Perspective. *Eur. J. Nucl. Med. Mol. Imaging* **2023**. [CrossRef]
67. Wit, E.M.K.; KleinJan, G.H.; Berrens, A.-C.; van Vliet, R.; van Leeuwen, P.J.; Buckle, T.; Donswijk, M.L.; Bekers, E.M.; van Leeuwen, F.W.B.; van der Poel, H.G. A Hybrid Radioactive and Fluorescence Approach Is More than the Sum of Its Parts; Outcome of a Phase II Randomized Sentinel Node Trial in Prostate Cancer Patients. *Eur. J. Nucl. Med. Mol. Imaging* **2023**. [CrossRef]
68. Frederiks, C.N.; Overwater, A.; Bergman, J.J.G.H.M.; Pouw, R.E.; de Keizer, B.; Bennink, R.J.; Brosens, L.A.A.; Meijer, S.L.; van Hillegersberg, R.; van Berge Henegouwen, M.I.; et al. Feasibility and Safety of Tailored Lymphadenectomy Using Sentinel Node-Navigated Surgery in Patients with High-Risk T1 Esophageal Adenocarcinoma. *Ann. Surg. Oncol.* **2023**, 1–10. [CrossRef] [PubMed]
69. Mulita, F.; Verras, G.-I.; Anagnostopoulos, C.-N.; Kotis, K. A Smarter Health through the Internet of Surgical Things. *Sensors* **2022**, *22*, 4577. [CrossRef] [PubMed]
70. Azargoshasb, S.; Boekestijn, I.; Roestenberg, M.; KleinJan, G.H.; van der Hage, J.A.; van der Poel, H.G.; Rietbergen, D.D.D.; van Oosterom, M.N.; van Leeuwen, F.W.B. Quantifying the Impact of Signal-to-Background Ratios on Surgical Discrimination of Fluorescent Lesions. *Mol. Imaging Biol.* **2022**, *25*, 180–189. [CrossRef] [PubMed]
71. Deken, M.M.; Bos, D.L.; Tummers, W.S.F.J.; March, T.L.; van de Velde, C.J.H.; Rijpkema, M.; Vahrmeijer, A.L. Multimodal Image-Guided Surgery of HER2-Positive Breast Cancer Using [(111)In]In-DTPA-Trastuzumab-IRDye800CW in an Orthotopic Breast Tumor Model. *EJNMMI Res.* **2019**, *9*, 98. [CrossRef]
72. Qin, Z.; Hall, D.J.; Liss, M.A.; Hoh, C.K.; Kane, C.J.; Wallace, A.M.; Vera, D.R. Optimization via Specific Fluorescence Brightness of a Receptor-Targeted Probe for Optical Imaging and Positron Emission Tomography of Sentinel Lymph Nodes. *J. Biomed. Opt.* **2013**, *18*, 101315. [CrossRef]
73. Gabriels, R.Y.; van Heijst, L.E.; Hooghiemstra, W.T.R.; van der Waaij, A.M.; Kats-Ugurlu, G.; Karrenbeld, A.; Robinson, D.J.; Tenditnaya, A.; Ntziachristos, V.; Gorpas, D.; et al. Detection of Early Esophageal Neoplastic Barrett Lesions with Quantified Fluorescence Molecular Endoscopy Using Cetuximab-800CW. *J. Nucl. Med.* **2023**, *64*. [CrossRef]
74. Gao, R.W.; Teraphongphom, N.; de Boer, E.; van den Berg, N.S.; Divi, V.; Kaplan, M.J.; Oberhelman, N.J.; Hong, S.S.; Capes, E.; Colevas, A.D.; et al. Safety of Panitumumab-IRDye800CW and Cetuximab-IRDye800CW for Fluorescence-Guided Surgical Navigation in Head and Neck Cancers. *Theranostics* **2018**, *8*, 2488–2495. [CrossRef]
75. Zhou, Q.; van den Berg, N.S.; Kang, W.; Pei, J.; Nishio, N.; van Keulen, S.; Engelen, M.A.; Lee, Y.-J.; Hom, M.; Vega Leonel, J.C.M.; et al. Factors for Differential Outcome Across Cancers in Clinical Molecule-Targeted Fluorescence Imaging. *J. Nucl. Med.* **2022**, *63*, 1693–1700. [CrossRef]
76. Zhang, Z.; Fang, C.; Zhang, Y.; Su, S.; Li, B.; Liu, G.; Hu, Z.; Tian, J. NIR-II Nano Fluorescence Image Guided Hepatic Carcinoma Resection on Cirrhotic Patient. *Photodiagnosis Photodyn. Ther.* **2022**, *40*, 103098. [CrossRef]
77. Sterkenburg, A.J.; Hooghiemstra, W.T.R.; Schmidt, I.; Ntziachristos, V.; Nagengast, W.B.; Gorpas, D. Standardization and Implementation of Fluorescence Molecular Endoscopy in the Clinic. *J. Biomed. Opt.* **2022**, *27*, 074704. [CrossRef]

78. Olympus CLV-S200-IR—Xenon Light Source: Product Details + Technical Specifications (PDF). Available online: https://www.olympus-europa.com/medical/en/Products-and-Solutions/Products/Product/CLV-S200-IR.html (accessed on 23 March 2023).
79. Food & Drug Administration Da Vinci Fluorescence Imaging Vision System, Da Vinci Firefly Imaging System. Available online: https://www.accessdata.fda.gov/cdrh_docs/pdf21/K213710.pdf (accessed on 23 March 2023).

Disclaimer/Publisher's Note: The statements, opinions and data contained in all publications are solely those of the individual author(s) and contributor(s) and not of MDPI and/or the editor(s). MDPI and/or the editor(s) disclaim responsibility for any injury to people or property resulting from any ideas, methods, instructions or products referred to in the content.